Research in Astronomy and Astrophysics, 22:035010 (12pp), 2022 March https://doi.org/10.1088/1674-4527/ac4702

New Features of the Pulsar B0950+08 Radiation at the Frequency of 111 MHz

V. M. Malofeev, I. F. Malov, O. I. Malov, and D. A. Teplykh
P.N.Lebedev Physical Institute of the Russian Academy of Sciences, Leninskii pr. 53, Moscow, 119991, Russia; teplykh@prao.ru
Received 2021 October 6; revised 2021 December 9; accepted 2021 December 13; published 2022 February 18

Abstract

Results of long time observations of the pulsar B0950+08 are given. These observations were carried out at the LPA radio telescope at the frequency of 111 MHz from January of 2016 to May of 2019 (450 days). A strong variability in emission of this pulsar has been detected with changes in signal to noise ratios hundreds of times. Part of the long-time flux density variability can be explained by refractive scintillations in the interstellar medium. The existence of radiation between the interpulse (IP) and main pulse (MP) was confirmed. It was more powerful than at high frequencies. We detected the unusual IP and precursor (Pr) radiation on 2017 August 1. On the basis of 65 strong IPs we found the correlations between energies of IP and Pr and between the phase of IP and the distance Pr–IP. It is shown that the observed peculiarities of this pulsar can be explained in the frame of the aligned rotator model. We estimated distances of radiation levels from the center of the neutron star. The calculated value of the initial period of 0.2 s means that not all pulsars are born with millisecond periods. The large age of the pulsar (6.8 million years) and the small angle between its magnetic moment and the rotation axis (less than 20°) confirm the suggestion related to pulsar evolution with respect to alignment.

Key words: (stars:) pulsars: individual (PST B0950+08) – radiation mechanisms: general – (stars:) pulsars: general

1. Introduction

Most of the known 3000-plus radio pulsars (Manchester et al. 2005) are characterized by an average pulse width of order several percent of the period. However, there are pulsars emitting in the wider longitude range. This is specific particularly for radiation at low frequencies. In this case emission is generated at large distances from the surface of the neutron star where the emission cone expands markedly. If the angle between the magnetic moment and the rotation axis is small then the line of sight can be inside the emission cone for a long time. We believe that such a case takes place for the pulsar B0950+08 emitting sometimes during the whole period. For example, such observations were made at 408 MHz (Hankins & Cordes (1981) and Perry & Lyne (1985)) and at 111 MHz (Smirnova 2012). Some features of this pulsar are discussed in our paper. In addition to the main pulse (MP) and interpulse (IP), this pulsar has the bridge and the precursor (Pr) located between MP and IP (see, for example, Hankins & Cordes (1981)). They analyzed the complex time-frequency structure of both integrated pulses and individual ones in this pulsar. The frequency dependences of the width of MP and IP as well as the distances between IP and MP were presented also. The discussion about the MP and IP arising from opposite magnetic poles or from a single magnetic pole (the aligned rotator) takes place in a number of papers (see, for example, Perry & Lyne (1985) and Hankins & Cordes (1981)).

The Large Phase Array (LPA) antenna was upgraded in 2014 and its sensitivity became two times higher. As a result, the time-frequency resolution was improved significantly and about 60 new pulsars and rotating radio transients (RRATs) were discovered (Tyul'bashev et al. 2016, 2017, 2018, 2020). There was the possibility to carry out new observations of the pulsar B0950+08 and detect some interesting features in its radiation. Further we describe the results of these new observations.

The remainder of the paper is organized as follows. In Section 2 we discuss some details of our observations. Section 3 contains the results and their analysis. In Section 4 the interpretation of these results and a discussion are given. In Section 5 the conclusions are summarized.

2. Observations

All observations were carried out using the meridional radio telescope LPA. Its antenna is the phased array composed of 16,384 dipoles. The geometric area of this antenna is more than 70,000 m^2 and the effective area is $47{,}000 \pm 2500\,m^2$ (Tyul'bashev et al. 2016). The antenna has 128 space beams with the size of one beam being $0.^{\circ}9 \times 0.^{\circ}5$. The duration of an observing session is $3.5/\cos\delta$ min, where δ is the decl. The measurement series, lasting about 10–20 days each, were carried out from 2016 to 2019. For the processing, 460 channels of the 512 channel digital receiver are utilized. The single channel bandwidth is 4.88 kHz, the time resolution is 1.23 ms and the total bandwidth is 2.245 MHz. All data are stored in a server. For the processing a special program has been developed (Malofeev et al. 2012). We have a rather good radio frequency interference (RFI) situation at our radio

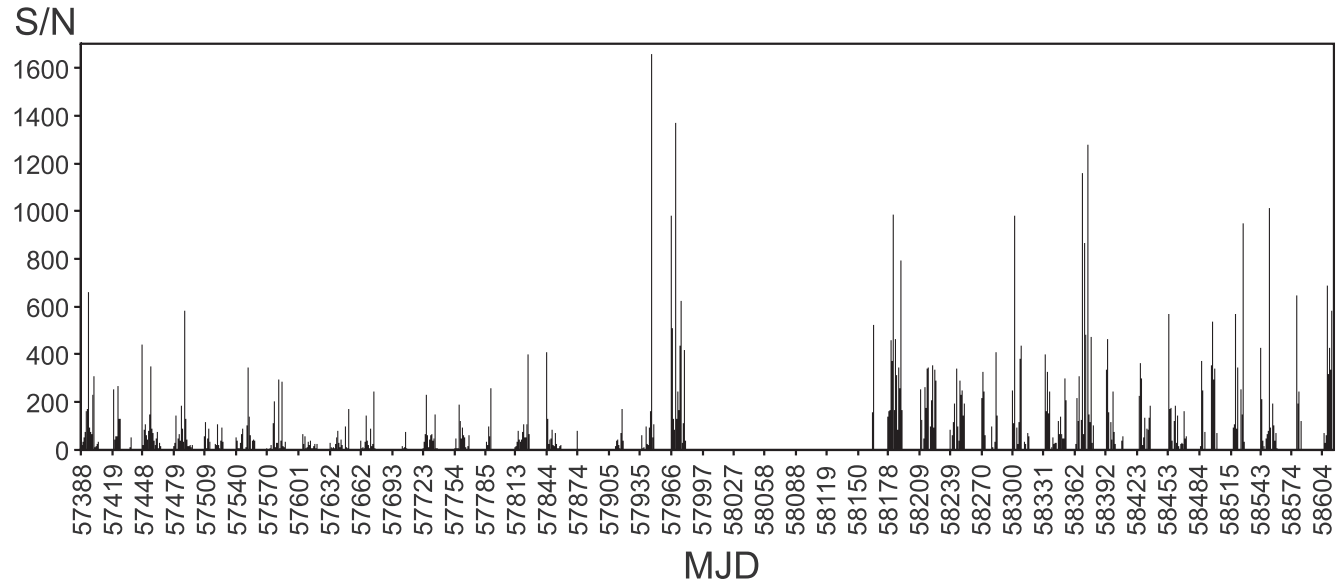

Figure 1. S/N variation of emission during 3.5 yr of observations.

telescope, especially during night time. We have the dynamic spectrum of every pulsar period and can detect a pulse of RFI in the frequency domain and in the time domain. There are two regular radio stations in our frequency band (2.245 MHz). They occupy 2–3 frequency channels (the band is equal to 10–15 kHz). Sometimes we see sporadic pulse RFI which occupies a part of our frequency band or even the entire band. To clean the data, we removed such frequency channels from the reduction. Our estimations show that the fraction of RFI data occupy no more than 2% of the observation time. Here we present the analysis of integrated profiles and single pulses for the pulsar B0950+08. The focus is on the unique event that took place on 2017 August 1.

3. Results and Analysis

Figure 1 shows the dependence of the signal to noise ratio (S/N) in integrated pulses on the date of observations from January of 2016 to May of 2019 (450 days). In our case, the value of S/N is the ratio of the pulse amplitude to sigma of the noise. To calculate σ we used the time interval with minimum radiation in the integrated profile of the pulsar. This interval is displayed in Figure 4(b).

It is evident that S/N or flux densities of integrated pulses are extremely variable. Integrated pulses were constructed on the basis of 3.2 minutes of observations (764 pulsar periods). These pulses change the intensities on the timescale from one to five days and show power bursts when S/N grows up to the value of 2000 in individual pulses. There are also long quasi-periodic variations of flux densities with scales of several months.

We detected the unusual changes of the flux densities of this pulsar on 2017 August 1. These changes took place on both millisecond scales inside the period (Figure 2) and second-minute scales (Figure 3) for the observation session duration of 3.2 minutes. Most likely these changes are caused by the radiation mechanism itself, however, some of them are possibly due to scintillations caused by inhomogeneities of the interstellar plasma.

3.1. Influence of Interstellar Scintillations and Polarization

There are two types of interstellar scintillations, namely, diffractive (DISS) and refractive (RISS) cases. The first ones are characterized by short periods, the second ones by long times. Shishov et al. (1995) published the empirical expressions for estimations of a decorrelation bandwidth ($\Delta\nu_d$), a decorrelation time (τ_d) and a scintillation index (m) describing diffractive scintillations. These expressions have been obtained on the basis of the large number of measurements for the parameters mentioned related to the number of frequencies for dozens of pulsars located at different distances or different dispersion measures, see the references in Shishov et al. (1995). We will utilize the following equalities

$$\Delta\nu_d(\mathrm{kHz}) = 8.8\left(\frac{\nu}{\nu_0}\right)^4\left(\frac{\mathrm{DM}}{\mathrm{DM}_0}\right)^{-1.45} \quad \text{for DM} \leqslant 20\ \mathrm{pc\ cm^{-3}} \tag{1}$$

and

$$\tau_d(\mathrm{min}) = 10\left(\frac{\nu}{\nu_0}\right)^{1.1}\left(\frac{\mathrm{DM}}{\mathrm{DM}_0}\right)^{-0.4} \quad \text{for DM} \leqslant 30\ \mathrm{pc\ cm^{-3}} \tag{2}$$

where $\nu_0 = 1$ GHz and $\mathrm{DM}_0 = 30\ \mathrm{pc\ cm^{-3}}$. Using $\mathrm{DM} = 2.97\ \mathrm{pc\ cm^{-3}}$ from Manchester et al. (2005) for the

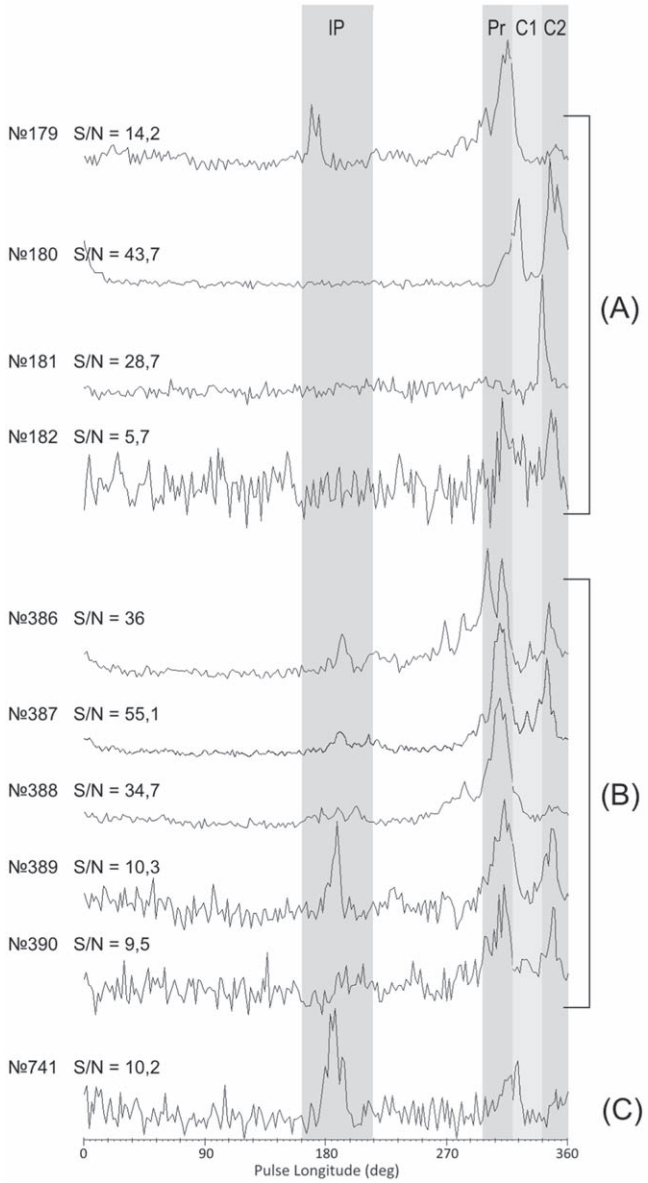

Figure 2. Examples of successive individual pulses on 2017 August 1.: changes of intensity for all components from one pulse to another (A), relative stability of radiation during several periods (B) and the case when IP is stronger than MP (C). The numbers of individual pulses are expressed.

pulsar B0950+08, we have $\Delta\nu_d = 38$ kHz and $\tau_d = 2.2$ minutes at the frequency of $\nu = 111$ MHz. Smirnova (2006) reported $\Delta\nu_d = 200$ kHz and $\tau_d > 3.3$ minutes. Using results of measurements at frequency of 60 MHz (Kuiack et al. 2020) and the value of $\Delta\nu_d = 32$ kHz at this frequency, we obtain 480 kHz for this quantity at our frequency based on Equations (1) and (2). Measurements of Bell et al. (2016) at 154 MHz give $\Delta\nu_d = 4.1$ MHz and $\tau_d = 28.8$ minutes. Then we have $\Delta\nu_d = 350$ kHz and $\tau_d = 21$ minutes at 111 MHz. Almost the same results are obtained if we use the dependences from Cordes (1986): $\Delta\nu_d = (\nu/\nu_0)^4$ and $\tau_d = (\nu/\nu_0)^{1.2}$. The scintillation index decreases markedly due to the smoothing of scintillations with the decorrelation bandwidth ~38 kHz inside of our receiver bandwidth (2.3 MHz). As was reported by Sutton (1971), the scintillation index decreases to 0.25 for the ratio of these two bands equal to 60. Hence, diffractive scintillations can not only explain millisecond and second intensity variations but also minute ones as well. Let us estimate the influence of refractive scintillations. For this process Shishov et al. (1995) obtained formulas for the scintillation index (m_r) and the decorrelation time (τ_r) on the basis of long time measurements by Gupta et al. (1993) at the frequency of 74 MHz

$$m_r = 0.6\left(\frac{\nu}{\nu_0}\right)^{1/2}\left(\frac{\mathrm{DM}}{\mathrm{DM}_0}\right)^{-1/3} \quad (3)$$

and

$$\tau_r(\mathrm{days}) = 40\left(\frac{\nu}{\nu_0}\right)^{-2}\left(\frac{\mathrm{DM}}{\mathrm{DM}_0}\right)^{1.5}. \quad (4)$$

As a result, we have $m_r = 0.42$ and $\tau_r = 101$ days. Let us compare these values with the results of measurements at fairly close frequencies. Gupta et al. (1993) published $m_r = 0.45$ and $\tau_r = 3^d.4$ at 74 MHz. Conversion to frequency of 111 MHz using Equations (3) and (4) gives $m_r = 0.55$ and $\tau_r = 1^d.5$. Bell et al. (2016) obtained $\tau_r = 20^h.9$ at 154 MHz. Conversion to 111 MHz leads to $\tau_r = 1^d.8$. Hence, the estimate of the refractive interstellar scintillation (RISS) from Equation (3) is very close to the corresponding value at 74 MHz. However, values of τ_r, obtained by Equation (4) differ by more than 50 times. This problem has been discussed already by Gupta et al. (1993). They predicted $\tau_r = 98^d$ using the equations valid for an extended medium model and a Kolmogorov spectrum without an inner scale (Rickett et al. 1984). This value differed by 30 times from the measured one of $\tau_r = 3^d.2$. The authors concluded that "It is not clear whether the results for PSR 0950 +08 are part of the same trend for the predicted RISS timescales to overestimate the observed values, or whether it presents a special case". Thus, we have two timescales for RISS at 111 MHz. Both scales are seen in our data (Figure 1). These scales are several days and several months. Perhaps we have to deal indeed with a special case in the direction of this pulsar. Hence, the observed variations of flux densities in the pulsar B0950+08 at the scales of order of a few days and months can be explained by RISS.

Analyzing intensity variations, we must take into account that the LPA radio telescope received radiation with a linear polarization. It is known that the position angle in the pulsar B0950+08 changes smoothly by 180° between MP and IP (Backer & Rankin 1980). A high degree of polarization is observed at frequencies lower than 200 MHz. For example, it is 67 ± 6 % at the frequency of 39 MHz (Suleimanova et al. 1983). The rotation measure of this pulsar is 4 rad m^{-2} and the

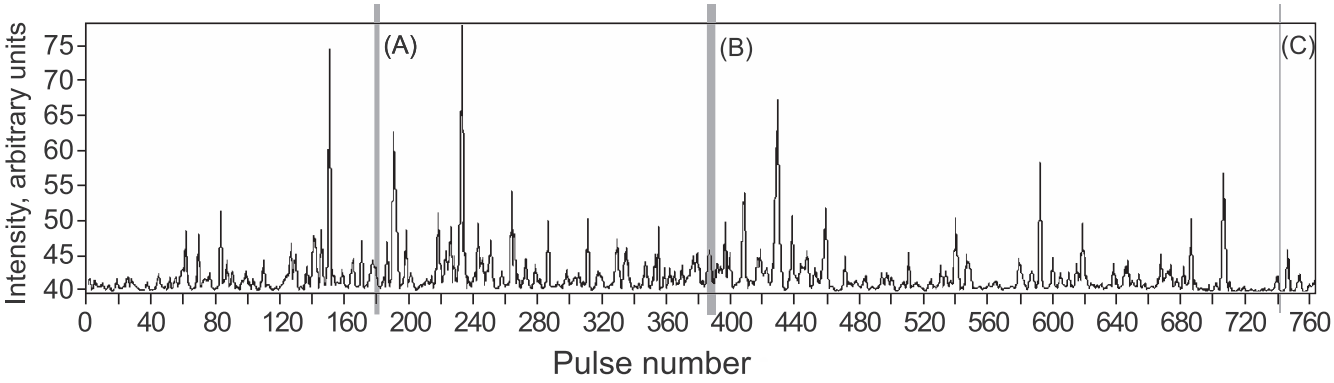

Figure 3. Relative intensity of radiation during the observation session on 2017 August 1. The gray blocks (A, B, C) are the pulses shown in Figure 2.

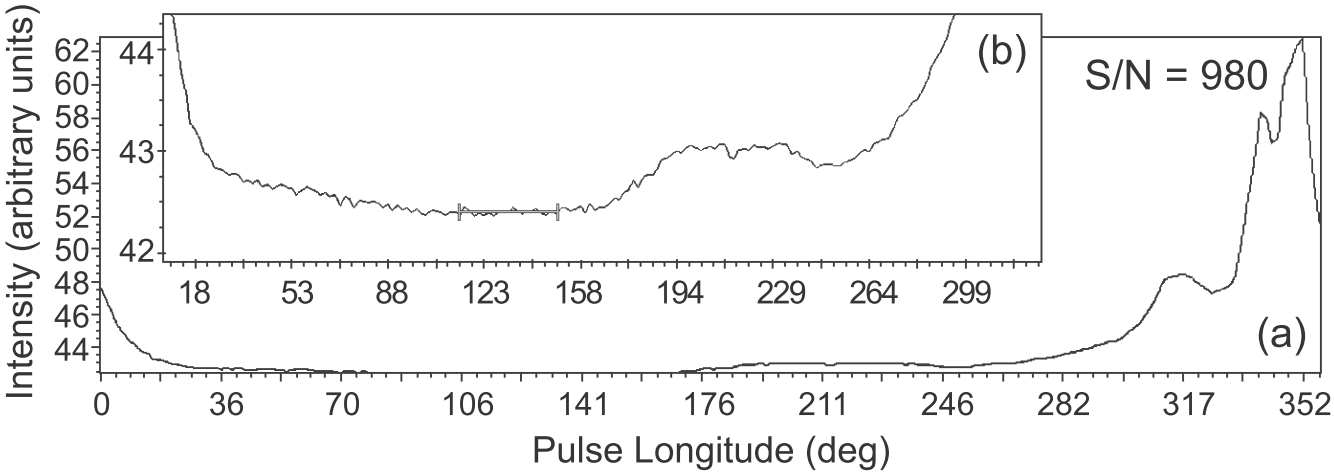

Figure 4. Integrated profile of PSR B0950+08 on 2017 August 1 (a) and outside the MP, 85% of the whole period at a scale of 10% of the amplitude of MP (b). The zero level is marked by the segment between 114° and 150° of the pulse longitude (b).

period of the intensity modulation due to the Faraday rotation is 6 MHz at the frequency of 111 MHz (Shabanova & Shitov 2004). Since the receiver bandwidth is 2.35 MHz, the angle of rotation is 70°. This leads to the noticeable and different intensity variations in two components of MP. Shabanova & Shitov (2004) demonstrated that the ratio of flux densities of these components could be up to two depending on the degree of linear polarization. Since the position angle between MP and IP changes approximately by 180°, the ratio of amplitudes of MP and IP must be unchanged for different observation days. However, intensities of the bridge and the Pr will change from day to day. We have analyzed the Pr (Figure 4), taking into account its high intensity of 29% compared to MP (2017 August 1, Table 1, Figure 4). The detailed description of errors for each considered component is given in Section 3.5. We have taken into account here one linear polarization of our antenna. The small sample of days with strong emission of the bridge does not allow us to make the detailed analysis of intensity variations of this feature. It is known that MP in this pulsar contains the orthogonal component manifested in the position angle (see, for example, Manchester et al. (1980)). This can explain the rear cases when we see IP and Pr but there is no MP (pulses 179 and 741 in Figure 2). Sometimes we observe only one component of MP, as a rule C2. Figure 2 features such cases.

3.2. Integrated Profiles

One of the main aims of our work was the detailed analysis of the pulsar emission for 2017 August 1. Let us compare the integrated profile of this day with other days. We constructed three groups by dividing them by their intensities. Pulses in the first group have on average $\langle S/N\rangle = 250$, for the second one $\langle S/N\rangle = 590$ and the third one is characterized by $\langle S/N\rangle \geqslant 1100$ (Table 1). Further we compare phases of MP and IP, their relative intensities, distances between MP and IP and their widths by the level 50%.

Table 1
Observed Intensities for Three Groups Mentioned

Data	S/N	Intensity of Pr in Relation to the MP (%)	Relative Intensity of IP/MP (%)
07.10.2018	225	3.9	<0.5
04.11.2018	297	7.0	1.0
03.01.2019	247	10.5	2.5
02.03.2019	211	5.0	<0.5
11.09.2018	481	2.6	2.5
01.12.2018	568	12.3	<0.5
04.12.2018	571	5.3	2.5
05.04.2019	648	5.9	1.2
05.05.2019	688	6.3	1.2
10.05.2019	585	2.7	2.5
13.07.2017	1656	9.6	0.8
01.08.2017	**980**	**29.0**	**3.5**
05.08.2017	1368	5.2	1.3
06.03.2018	984	8.2	0.8
14.03.2018	795	3.4	1.8
03.07.2018	982	2.8	1.0
07.09.2018	1159	3.2	0.7
13.09.2018	1276	11.1	0.8
12.02.2019	948	16.8	<0.5
10.03.2019	1014	7.3	2.3

Figure 4(a) displays the integrated profile for 2017 August 1 (sum of 764 pulses). This day was unique among all 450 observation days. The pulsar emitted practically during all time (see, for example, some successive pulses in Figure 2). Perry & Lyne (1985) and Hankins & Cordes (1981) gave the integrated profile of the pulsar B0950+08 at the frequency of 408 MHz and declared that emission was observed almost during the entire period (83%) and individual IPs were occasionally as strong as 60% of the average MP. It follows from Figure 4(b) demonstrating 85% of the whole period without the MP and drawn at a scale of 10% of the amplitude of MP that the interpulse emission (IP and the bridge) is on average at least 2.5% of the MP intensity and this radiation occupies about 90% of the entire period. Figure 4 shows clearly that the IP emission passes smoothly into the bridge and then through the Pr into MP. A similar effect was noted earlier by Smirnova & Shabanova (1988) at the frequency of 102.5 MHz, but their estimate was approximately two times lower (1.3%). Since our estimate has been obtained on the whole period but not at the specific phase inside it, we assert there is a much more intense effect. Moreover, this estimate exceeds the mean level for all three groups mentioned earlier (Table 1). As can be seen from this table, the increase of the MP intensity correlates with the decrease of the intensities for Pr and IP. Comparison of intensity on 2017 August 1 with other days shows that it is several times higher than S/N for the third most powerful group.

It is worth noting that in the pulsar considered it is difficult to determine the level where there is no radiation (Hankins & Cordes 1981). We took for the zero level an area with minimum radiation intensity. The duration of zero longitudes is 36° for all days. The zero level is shown in Figure 4(b).

3.3. Individual Pulses

Strong jumps in intensity have been observed on 2017 August 1 both in the separate components of MP and in the IP space. Figure 2 displays a series of individual successive pulses for this day. The central part of the window contains IP. This feature can be as strong as MP (Figure 2(B), 389) and even stronger than MP (Figure 2(C), 741).

As a rule, the structure of pulses and their intensity change sharply from one pulse to another (see Figure 2(A), where four successive pulsar periods are illustrated). However, sometimes radiation is stable during 3–4 periods (Figure 2(B)). As for the IP emission, it changes markedly from one period to another. In Figure 2 gray blocks indicate the phase boundaries of the components relative to the integral form (Figure 4). These are: IP = 175°–230°, Pr = 300°–323° and MP = 324°–360° with the boundary between C1 and C2 at the phase of 342°. All series of pulses are marked by the gray blocks in Figure 3. The interval of our observations (13.07.2017–10.03.19) is inside of the interval of observations of this pulsar using LOFAR at the frequency of 60 MHz (Kuiack et al. 2020). They demonstrate that the flux density increased in 2018 compared to 2017. A similar effect has been observed at our frequency of 111 MHz as well (see Figure 1). Moreover, at 60 MHz 275 giant pulses (GPs) were detected during 90 hr of observations, that is three GPs per hour. Tsai et al. (2015) detected five GPs during one hour of observations at 39 MHz. At our frequency, about 250 strong pulses were also detected by Smirnova (2012) during one hour of observation. However, it is not clear that can we consider these pulses as GPs. Singal & Vats (2012) declared that about 1% of pulses at 103 MHz are GPs. We found no GP during 20 days (64 minutes) of observations (Table 1). Such large discrepancy in the rate of GPs at close frequencies can be explained by the strong day-to-day variation of this rate (Singal & Vats 2012).

As can be seen from Figure 2, some individual pulses can produce emission during the whole period of the pulsar. The maximal value of S/N for one of the individual MPs is more than 2000. The mean value of S/N is 980. We carried out the quantitative analysis of the individual behavior of IP, Pr and MP for each of 20 days as given in Table 1.

3.4. Main Pulse

To find out how unique the day of 2017 August 1 is, we construct three groups of integrated pulses with different values of S/N. They are listed in Table 1. The first group corresponds to 4 days of observations, the second one to 6 days and the third to 10 days. All 20 days are inside the interval between 2017 July 13 and 2019 May 5. First of all we counted numbers of individual pulses in nine intervals of S/N from $S/N \geqslant 5$ to

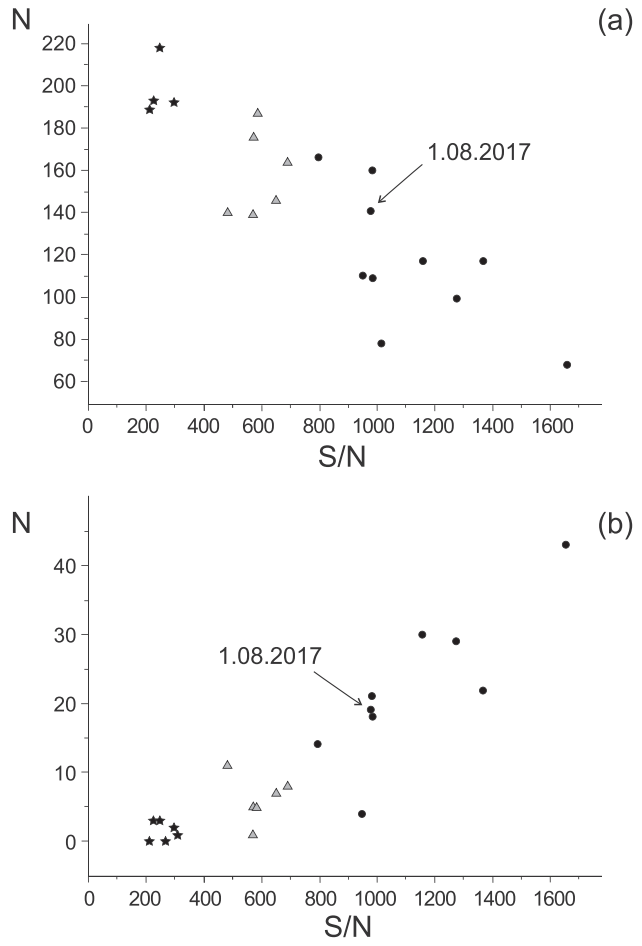

Figure 5. Numbers of individual pulses for S/N = 5–10 (a) and S/N = 320–640 (b). The mean S/N ratio is displayed on the abscissa (see Table 1). Three groups of days from Table 1 are shown by different marks: the first group by asterisks, the second one by gray triangles and the third one by circles.

S/N ⩾ 1280, and for each next interval S/N is two times higher. Then we analyzed dependences of these numbers on S/N in integrated pulses for all nine intervals. Figure 5 displays the dependences for two intervals. It is confirmed that for small values of S/N (Figure 5(a)) the number of pulses decreases with the growth of S/N. For strong pulses (S/N = 320–640) the dependence is opposite. There is not a correlation for intermediate values of S/N.

We analyzed differential distributions of pulse numbers for each range of values of S/N. The maximum of the distribution for the first weak group corresponds to S/N ⩾ 5–10, and 66% of pulses have amplitude with S/N ⩾ 5. In the third strong group the maximum of the distribution is located in the range S/N ⩾ 10–40, and the total fraction of visible pulses is of order of 90%. Hence, an amplitude of an integrated pulse depends not only on the number of individual pulses with an amplitude greater than the specified one but also on the intensity of these pulses.

3.5. Interpulse, Precursor and Main Pulse

The unique day 1.8.2017 is located in the middle of the strong integrated pulses (the third group) in Figure 5. However, the maximal value of the IP and Pr amplitudes were recorded just on 1.8.2017 both in the integrated profile and in individual pulses. Smirnova (2006) analyzed the Pr and MP at the frequency of 111 MHz and then searched for giant pulses in this pulsar. We give detailed analysis of IP and its connection with Pr and MP for the first time. We analyzed four components of individual pulses, namely, IP, Pr, C1 and C2 of MP. The following parameters of these components have been investigated: phases, amplitudes, durations at level 50% and integrated energies. Besides, we considered the energy of the previous MP, since Hankins & Cordes (1981) found the connection of this component with IP. These parameters are listed in Table 2. Most of our flux density measurements were made using the discrete calibration sources and the calibration signal, which was recorded synchronously at the beginning of every period of the pulsar. Such method was applied earlier for the measurements of flux densities for 235 pulsars at 102.5 MHz (Malofeev et al. 2000). In the present work we tried to investigate the pulsar profile during the entire period without any calibration signal. Therefore, we used new LPA pulsar flux calibration hardware and software, described in Tyul'bashev et al. (2016, 2020). Daily measurements of the noise flux densities, using six calibration sources, were carried out. The calibration signal was recorded in the form of OFFONOFF. The temperatures of ON and OFF signals were 2400 K and ∼300 K, respectively. Sigma of noises was calculated in the interval with minimum radiation in the pulsar period (Figure 4(b)). We obtained $\sigma = 1.3 \pm 0.2$ Jy, with the parameters of observations: time resolution—1.23 ms and the total bandwidth—2.245 MHz. The processing of data gave S/N for single pulses and we can calculate the energy of all components. In Table 2 all 65 individual pulses with S/N more than 4 are collected. The first column contains the pulse numbers. From the second column to the fifth one we give phases of four components. The sixth and seventh ones present phase differences D with their errors (in brackets). The eighth column shows which component value of D was calculated, when the amplitudes of components C1 and C2 were not equal. For example, there are pulses 386 and 387 (Figure 2(b)), where we can see component C2 only. From the ninth column to the twelfth one energies are given. Figure 6 features the distributions of phases for all four components. We can note two features in these distributions. First, three components (Pr, C1 and C2) can be approximated by Gaussians. Second, the size of the distribution for IP is approximately equal to the total size of the Pr+MP distribution. We search for connections between IP and other components (Pr, MP, and separately C1 and C2). More than 20 paired relationships between parameters of different components (phases, amplitudes, durations and

Table 2
Characteristics of Some Components of Individual Pulses

Pulse Number	Phase (deg)				D (deg)		Component of MP	Energy (Jy ms)			
	IP	Pr	C1	C2	Pr–IP	MP–IP		IP	Pr	MP	MP_{prev}
85	199	317	343		118(2)	144(5)	C1	92	169	130	43
93	215										
109	191	311		350	120(2)	159(5)	C2	184	268	256	180
128	198	313	338	352	115(6)	154(6)	C2	107	152	450	2454
145	206	313	338	360	107(4)	143(4)		79	238	246	
146	198	313	338	352	115(1)	147(6)		500	390	2231	246
177	195	317		350	122(2)	155(5)	C2	346	346	253	383
178	188	305		359	117(4)	171(6)	C2	114	823	453	253
179	178	318			140(3)			113	478	293	453
191	191	324		348	133(5)	157(3)	C2	117	673	6593	466
211	205	315		355	110(3)	150(7)	C2	376	376	167	83
214	196	319		355	123(4)	159(6)	C2	120	250	496	153
224	207	317		347	110(3)	140(6)	C2	266	150	929	1692
228	189	319	340	348	130(4)	159(5)	C2	133	316	2850	186
232	205	321	336	352	116(3)	139(5)		242	827	3926	1765
248	195	305	336	352	110(3)	149(5)		103	120	509	120
250	217	315	340	352	98(3)	129(3)		30	333	260	473
271	204	306		347	102(3)	143(3)	C2	58	152	87	67
273	198	315		350	117(3)	152(5)	C2	225	225	1136	413
300	220	313			93(2)			170	40		1462
301	187	318		354	131(3)	167(4)	C2	83	92	100	
341	200	317	343		117(3)	143(4)	C1	47	87	47	17
346	193	308		360	115(1)	167(3)	C2	85	180	40	73
374	208	315		352	107(3)	144(4)	C2	133	549	226	
379	177	313	334	357	136(4)	169(5)		65	300	719	541
386	199	308		353	109(4)	154(3)	C2	157	616	133	67
387	207	313		348	106(3)	141(4)	C2	260	866	450	133
388	193	313		356	120(2)	163(7)	C2	300	842	120	450
389	195	317		354	122(4)	159(4)	C2	55	233	117	120
391	215	308	343	354	93(5)	134(5)		63	400	563	25
392	187	312	333	354	125(3)	151(6)		93	493	799	563
394	208	317		358	109(2)	150(5)	C2	133	290	260	266
408	220	310	331	348	90(1)	128(6)	C2	45	653	2045	390
416	228	305		353	77(2)	125(4)	C2	107	210	80	60
428	200	310	340	352	110(2)	146(5)		186	1865	346	1941
429	222	312	338	354	90(3)	124(5)		2198	4928	1399	3468
430	200	322	336	350	122(5)	136(4)		433	3040	2957	1399
431	208	312		350	104(2)	142(5)	C2	1432	1332	80	2957
432	226	318		358	92(3)	132(3)	C2	55	373	653	80
438	210	313	338	357	103(2)	138(6)		133	403	706	
441	208	315		361	107(2)	153(4)	C2	112	216	390	346
442	189	311	333	357	122(2)	152(5)		310	350	53	390
444	205	308		352	103(2)	147(3)	C2	60	646	286	57
447	201	317	338	352	116(3)	144(5)		160	320	2338	193
457	199	315		359	116(3)	160(4)	C2	230	1439	67	140
473	200	322		355	122(2)	155(5)	C2	93	230	30	
483	184	308	329	355	124(2)	158(4)		93	133	326	453
494	192	320	342	359	128(3)	159(4)		93	226	763	
497	198	310		355	112(4)	157(4)	C2	120	293	147	120
508	193	322	337	355	129(4)	153(4)		64	85	38	130
533	205	310	334	355	105(3)	140(5)		100	110	70	
549	192	308		355	116(3)	163(4)	C2	130	882	253	40
579	227	315	336	352	88(2)	117(4)		158	250	504	90
601	190	305	332		115(4)	142(5)	C1	117	157	53	1758
621	204	306	339	350	102(3)	141(5)		9	173	370	706
647	213	322	334	354	109(2)	131(2)		117	113	455	460
658	213	320		361	107(1)	148(3)	C2	60	117	67	24

Table 2
(Continued)

Pulse Number	Phase (deg)				D (deg)		Component of MP	Energy (Jy ms)			
	IP	Pr	C1	C2	Pr–IP	MP–IP		IP	Pr	MP	MP_{prev}
667	193	317	341	353	124(2)	154(3)		47	120	653	60
669	203	317		353	114(3)	150(2)	C2	45	306	47	1605
674	202		341	350		144(3)		93		1382	554
678	195	313	340	355	118(2)	152(3)		18	140	140	
704	206							47			73
705	205	313	339	349	108(2)	139(5)		40	266	546	
741	194	324				130(2)		886	117		93
754	187	315	331	354	128(2)	155(3)		80	526	167	67

energies) were analyzed. A strong inverse correlation between the phase of IP and the difference D of phases (Pr–IP) has been detected (Figure 7(a)). The correlation coefficient for 62 pairs is $K = -0.92$. The probability of a random distribution in Figure 7(a) $p < 0.0001$. The linear approximation of the relationship in Figure 7(a) can be described by the following equation

$$D = (-1.02 \pm 0.06)\text{Phase(IP)} + (318 \pm 11). \quad (5)$$

There is also the inverse dependence between phases of IP and MP–IP (Figure 7(b)). It shows a high correlation coefficient $K = -0.85$ and the probability of a random distribution $p < 0.0001$. It is very important to know which component is connected with IP. We conclude that this is Pr. First, we can see (Table 1, Figure 4) that the intensity of Pr in the integral pulse on 01.08.2017 is much higher than during other days and is about 29% of MP. Second, when IP appears Pr, as a rule, is observed also (62 cases among 65 ones) (Table 2). At the same time, we only see 57 C2 and 32 C1. Figure 2 demonstrates clearly that all seven pulses have IP and Pr simultaneously, and there are only four MPs at the same time. Third, there are positive correlations between energies of different components (Figure 8). For 62 pairs of Pr and IP we obtained

$$\log E(\text{Pr}) = (0.48 \pm 0.11)\log E(\text{IP}) + (1.49 \pm 0.24), \quad (6)$$

with the correlation coefficient $K = 0.49$ and the probability of a random distribution $p < 0.0001$. For two other relationships we have for 60 pairs of MP and IP $K = 0.17$, $p = 0.18$, and for 55 pairs of IP and the previous MP $K = 0.26$, $p = 0.05$.

We have calculated similar relationships for three other days (11.09.2018, 10.03.2019 and 10.05.2019) with intensities of IP more than 2.3% compared to MP (Table 1). The total number of Pr–IP pairs was equal to 23. The mean value of the correlation coefficient ($9\langle K\rangle = 0.44$) is very close to the mentioned value of $K = 0.49$ for 01.08.2017. For 53 IP-subsequent MP pairs $K = 0.30$, and for 52 IP-previous MP pairs $K = 0.36$. These values are somewhat higher than $K = 0.26$ for 01.08.2017. It is important to note that obtained values of it (0.26 and 0.36) for IP-previous MP pairs are close to the values from Hankins & Cordes (1981), where this quantity changes from 0.14 to 0.34 for three series counting 200 pulses.

Let us discuss the problem of energy measurement errors taking into account the registration of signals by the linearly polarized antenna As follows from Section 3.1, IP and MP are 150 degrees apart and have the same phase of the position angle (the difference is equal to 180 deg.). However, paying attention to the rather wide distributions of phases for different components of pulses (Figure 6), we must take into account the corresponding changes of position angles when estimating errors in values of energy. We have estimated the mean statistical errors of the measured values of energy. These are for IP $\varepsilon = \frac{22^\circ}{75^\circ} \times 70\% = 21\%$ and for MP $\varepsilon = \frac{25^\circ}{75^\circ} \times 70\% = 23\%$. Here 22° and 25° are the widths of IP and MP distributions respectively, and 75% is the part of the period where the changes in the position angle are equal to 90°. The degree of pulsar linear polarization is 70% at our frequency (see Section 3.1). The situation is not so clear for the IP–Pr pair. If we suggest that the Prs are on average 112° apart from IPs (Figure 6), then the error of the measured energy in Pr consists of two quantities. The first one is caused by the phase variations for Pr $\frac{12^\circ}{75^\circ} \times 70\% = 11\%$, and the second by the difference in position angles of these two components $\frac{112^\circ - 75^\circ}{75^\circ} \times 70\% = 35\%$. These errors are independent and their mean is $37\% = (11^2 + 35^2)^{1/2}$. Also, there are errors is measurements of energy itself caused by noises. This one is no more than 15%. Therefore the total errors in energy are 26% for IP and 28% for MP. The error is equal to 40% for Pr. We do not know the position angle location for the IP–Pr pairs during our observations and have taken the mean value of the error for both components as $\frac{26\% + 40\%}{2} = 33\%$. We present three relationships between energies of IP–Pr, IP–MP and IP-previous MP in Figure 8. We do not show errors. They greatly burden the presented pictures, but do not change the obtained dependences and values of the correlation coefficients.

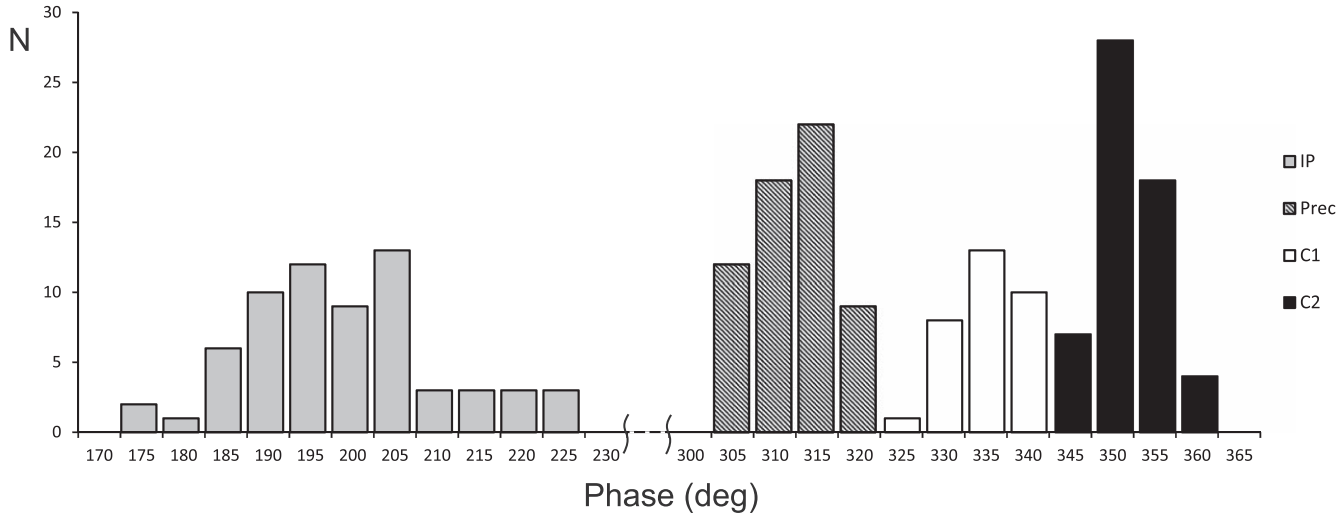

Figure 6. Distributions of phases for IP, Pr, C1 and C2.

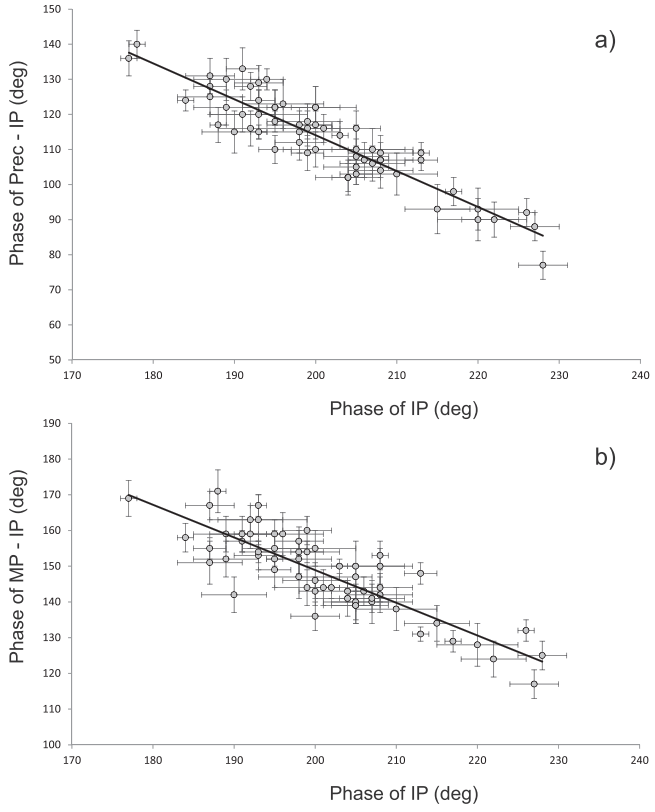

Figure 7. Relationship between phases of IP and Pr (a); between IP and MP (b).

We can conclude that there are correlations both between intensities of IP and Pr and between their phases. This picture reminds us of the complex relationship between the IP and the second component of the MP in the pulsar B1822-09 (Gil et al. 1994) where the correlations between spectra and durations of these features have been detected.

4. Discussion

Hankins & Cordes (1981) listed the following arguments for the assumption that pulsar B0950+08 is an aligned rotator. (1) There is emission between MP and IP. (2) There is a correlation between intensities of MP and IP. (3) The distance between MP and IP differs from 180°. (4) The position angle of linear polarization changes smoothly from MP to IP. (5) The microstructures in MP and IP have similar timescales: 130 μs in MP and 90 μs in IP (Backer et al. 1973). We believe that these arguments exclude the possibility of a description of observed peculiarities in the frame of the orthogonal rotator model. Malov & Nikitina (2013) estimated values of the angle β between the magnetic moment and the rotation axis in the pulsar B0950+08 by several methods and gave the mean value of this angle $\langle \beta \rangle = 18.^{\circ}9$. For the angle between the rotation axis and the line of sight they obtained $\zeta = 6.^{\circ}7$. For these angles the model path of the position angle of linear polarization is in good agreement with the observed one. Earlier similar values of these angles have been obtained by Narayan & Vivekanand (1983), namely $\beta = 10^{\circ}$ and $\zeta = 5^{\circ}$. An indirect argument for the aligned rotator in the case of PSR B0950+08 is its age. Malov & Nikitina (2013) demonstrated that orthogonal rotators had ages several times less than aligned ones. The investigated pulsar is located far enough from the Galactic plane, and its height is $z = 0.18$ kpc. The low radio luminosity of this pulsar ($L = 27.41$ m Jy kpc^2) shows also that it is a decaying source. Moreover using its transverse velocity $V = 36.55$ km s^{-1} (Manchester et al. 2005) and suggesting that its movement is isotropic, i.e., $V_z = 25.84$ km s^{-1}, we can estimate its kinematic age as $\tau = z/V_z = 6.8$ million years. This means that it is an old pulsar. Suggesting that the braking of the pulsar at the constant rate $dP/dt = 2.3 \times 10^{-16}$ (Manchester et al. 2005) and its real age equals to the kinematic one, we can estimate its initial period obtained at the moment of its birth as

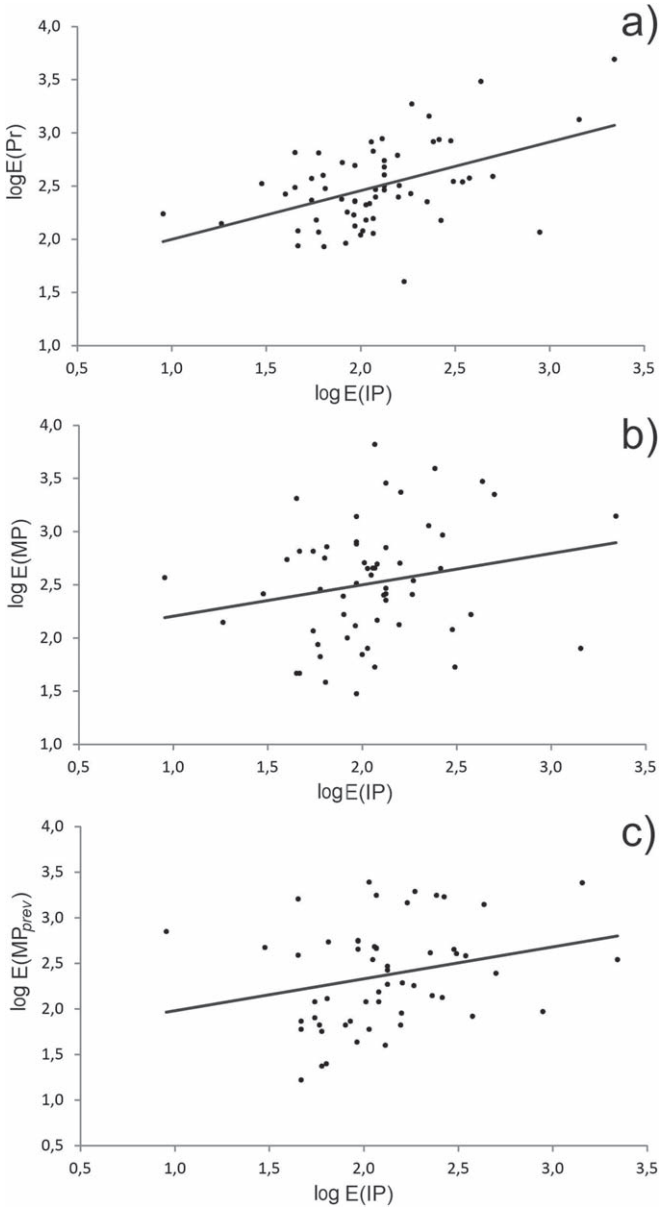

Figure 8. Relationship between energies of Pr and IP (a); MP and IP (b); previous MP and IP (c).

$P_0 = P - \tau dP/dt \approx 0.2$ s. This means that the pulsar B0950+08 was born as a long periodic object, and that not all pulsars were born with millisecond periods. If PSR B0950+08 is a typical object among pulsars we can conclude that old pulsars have small values of angle β and, hence, these angles decrease with age. Such a conclusion was made earlier by Malov (1990) and by Philippov et al. (2014).

The possible geometry explaining the peculiarities of observed emission is displayed in Figure 9. We use further values $\beta = 18.^{\circ}9$ and $\zeta = 6.^{\circ}7$. Some active areas (spots) can exist in the polar cap of a pulsar. They are formed as a result of surface sparking causing the generation of an unsteady electric field (Ruderman & Sutherland 1975). Their radiation then spreads through the narrow columns with angular sizes increasing away from the surface of the neutron star. It is variable due to changes with time of concentrations and energies of emitting charges. Such a variability reveals itself in sharp changes of all observed components (MP, IP, Pr and emission between them). At low frequencies the MP consists of two components, and at enough high ones one of them is out of sight. The angular distance between MP and IP can remain unchanged if the location of the spots mentioned is not changed.

We suggest here that the generation of emission at the chosen distance from the center of the neutron star occurs at the local plasma frequency

$$\nu_p = \left(\frac{2n_p e^2}{\pi m}\right)^{1/2}, \quad (7)$$

where n_p is the concentration of the secondary electron–positron plasma. Let us suggest that during the cascade process of the plasma birth, all energy of the primary beams is transferred to new electrons and positrons

$$\gamma_b n_b mc^2 = 2\gamma_p n_p mc^2. \quad (8)$$

Here γ_b and γ_p are Lorentz-factors of the primary particles and the newly born electrons, respectively, and

$$n_b = \frac{B}{Pce} \quad (9)$$

is the concentration of charges in the primary beam (Goldreich & Julian 1969).

For the dipolar magnetic field we have

$$\nu_p = 2.37 \times 10^3 \left(\frac{B\gamma_b R_*^3}{P\gamma_p r^3}\right)^{1/2}. \quad (10)$$

Substitution of $P = 0.253$ s and magnetic field at the magnetic pole, which is two times higher than the value of $B = 2.44 \times 10^{11}$ G from the ATNF catalog (Manchester et al. 2005), and using values of $\gamma_b = 10^7$ and $\gamma_p = 100$ give

$$\nu_p = 10^{12}\left(\frac{R_*}{r}\right)^{3/2}. \quad (11)$$

We calculated distances where emissions at frequencies 1400 and 111 MHz are generated: $\left(\frac{r}{R_*}\right)_{1400} = 90$, $\left(\frac{r}{R_*}\right)_{111} = 489$.

The light cylinder radius $r_{\rm LC} = \frac{cP}{2\pi}$ is 1.2×10^9 cm $= 1200\, R_*$ for pulsar B0950+08. The equation for the last open field lines in the dipole geometry is

$$\frac{r}{\sin^2\theta} = r_{\rm LC}. \quad (12)$$

They form the emission cone in the frame of the polar cap model. Equation (12) determines the angular radii of this cone

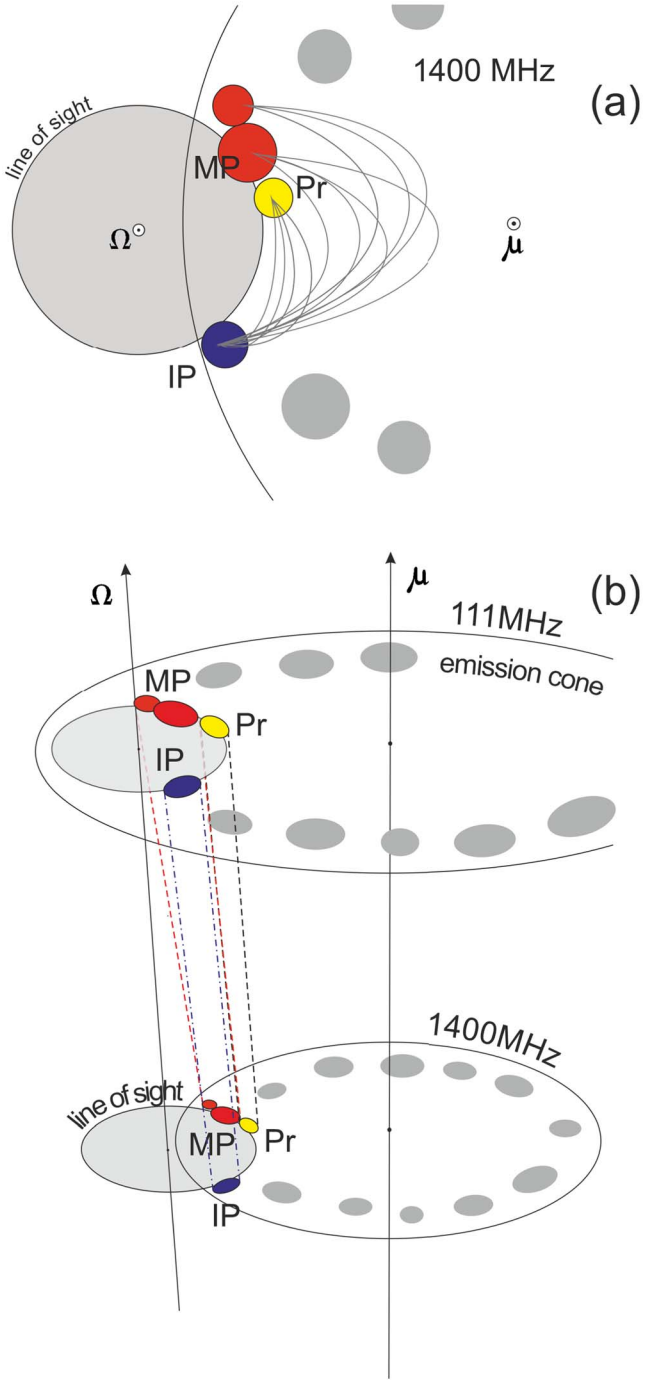

Figure 9. The proposed explanation of the obtained dependences between parameters of MP and IP at two frequencies in the frame of the single pole model. (a) Relative distribution of spots at the surface of the neutron star, rotation (Ω), magnetic axes (μ) and line of sight at the level where radiation at the frequency of 1400 MHz is generated are shown. Axes Ω and μ are perpendicular to the plane of the figure. (b) MP and IP emission is generated in the cones connected with some spots. Here it was assumed that the angle between the magnetic moment and the rotation axis $\beta = 18.^{\circ}9$ and between the line of sight and the rotation axis $\zeta = 6.^{\circ}7$. For clarity, the angular size of the top cone is shown not on the same scale.

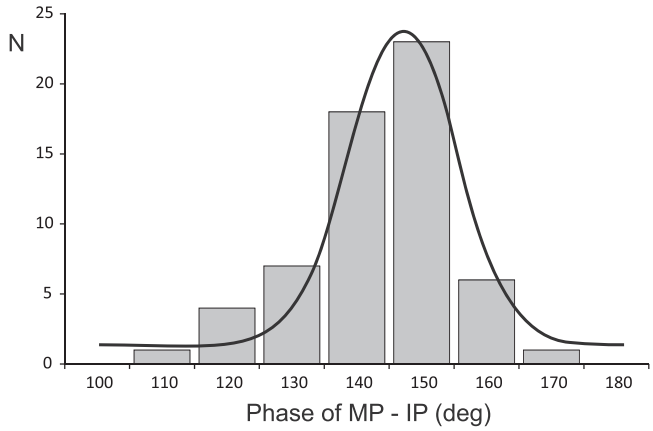

Figure 10. Distribution of observed distances between IP and MP.

at the calculated levels: $\theta_{1400} = 15.^{\circ}9$, $\theta_{111} = 39.^{\circ}7$. These values have been used in Figure 9.

Our observations show noticeable variations in the distance between IP and MP (Figure 10).

The maximum of the distribution of D = IP–MP is $146.^{\circ}5$, and this distribution can be described well by the following Gaussian

$$N = 24 \exp\left\{-\left(\frac{146.5 - D}{16.4}\right)^2\right\}. \quad (13)$$

Variations of D, the wide distribution of this distance and the mentioned difference from 180° are strong additional arguments in favor of the alignment of this pulsar. These are mentioned here for the first time. For an orthogonal rotator D must be very near 180° with minor deviations from this value. Variability in aligned objects can be caused by different intensities of separate parts of corresponding spots and by their movement on the surface of a neutron star caused by oscillations of the surface and waves spreading over it. Figure 9 shows how we can reconcile our model with the observed dependences of features in MP and IP on frequency given by Hankins & Cordes (1981).

In our model, distances between sub-pulses of MP are determined by the structure of magnetic field lines in spots (Figure 9(a)). At high frequencies near the surface of the neutron star this distance is almost constant. When we move away from the surface field lines diverge, the angular radius of the emission cone increases and the distance between sub-pulses also increases. This effect explains similarly the width of MP at different frequencies. At some distance from the neutron star one of the spots is out of sight and one of the components becomes invisible. The width of MP changes abruptly at higher frequencies and is determined by the width of the remaining component. The distance between IP and MP, as described earlier, is determined by the almost unchanged distance between the corresponding spots. They are connected by

magnetic field lines (see Figure 9), and this explains the weak radiation at longitudes between MP and IP.

5. Conclusions

Some results of long-term observations of the pulsar B0950 +08 using radio telescope LPA at the frequency of 111 MHz are given.

A strong variability in the intensity was revealed in radiation of the pulsar showing changes in the S/N of hundreds of times at different timescales. This variability is caused mainly by peculiarities in the emission mechanism. However, long-term fluctuations with the characteristic time of several days and months can be explained by RISS in the interstellar medium.

Analysis of the integrated profile of MP shows that the amplitude of its radiation depends on both number of pulses and their intensities. The existence of radiation between IP and MP has been confirmed. It is more intense compared to the higher frequencies. We carried out a detailed analysis of the unique event on 1.08.2017 showing strong radiation in almost the whole IP space.

We detected high correlations both between changes in intensities of Pr and IP and between phases of IP and Pr. New peculiarities of the pulsar emission such as the correlation between parameters of IP and Pr, the rather wide distribution of IP phases and distances between IP and MP can be explained in the frame of the aligned rotator model. The empirical version of such a model of the pulsar magnetosphere is proposed. We believe that there are some spots at the surface of the central neutron star in the pulsar B0950+08. They determine the structure of emission cones at different frequencies. Particularly, such a model explains qualitatively the complex picture of emission at low frequencies and gives the possibility to calculate distances where the observed emission is generated.

We also estimated the initial period of the pulsar acquired at birth ($P_0 \approx 0.2$ s). This means that not all pulsars are born with millisecond periods. The large age of the pulsar (6.8 million years) and the small angle between the magnetic moment and the rotation axis are evidences of the evolution of pulsars to aligned rotators.[1]

Acknowledgments

The authors thank T. V. Smirnova for the useful discussions and S. V. Logvinenko for the technical support of observations and data processing.

References

Backer, D., Boriakoff, V., & Manchester, R. 1973, NPhS, 243, 77
Backer, D., & Rankin, J. 1980, ApJ, 42, 143
Bell, M., Murphy, T., Johnston, S., et al. 2016, MNRAS, 461, 908
Cordes, J. 1986, ApJ, 311, 183
Gil, J., Jessner, A., Kijak, J., et al. 1994, A&A, 282, 45
Goldreich, P., & Julian, W. 1969, ApJ, 157, 869
Gupta, Y., Rickett, B., & Coles, W. 1993, ApJ, 403, 183
Hankins, T., & Cordes, J. 1981, ApJ, 249, 241
Kuiack, M., Wijers, R., Rowlinson, A., et al. 2020, MNRAS, 497, 846
Malofeev, V., Teplykh, D., & Logvinenko, S. 2012, ARep, 56, 35
Malofeev, V. M., Malov, O. I., & Shchegoleva, N. V. 2000, ARep, 44, 436
Malov, I. 1990, SvA, 34, 189
Malov, I., & Nikitina, E. 2013, ARep, 57, 833
Manchester, R., Hobbs, G., Teoh, A., & Hobbs, M. 2005, AJ, 129, 1993
Manchester, R. N., Hamilton, P., & McCulloch, P. 1980, MNRAS, 192, 153
Narayan, R., & Vivekanand, M. 1983, ApJ, 274, 771
Perry, T., & Lyne, A. G. 1985, MNRAS, 212, 489
Philippov, A., Tchekhovskoy, A., & Li, J. 2014, MNRAS, 441, 1879
Rickett, B. J., Coles, W. A., & Bourgois, G. 1984, A&A, 134, 390
Ruderman, M. A., & Sutherland, P. G. 1975, ApJ, 196, 51
Shabanova, T., & Shitov, Y. 2004, A&A, 418, 203
Shishov, V., Malofeev, V., Pinzar', A., & Smirnova, T. 1995, ARep, 39, 428
Singal, A., & Vats, H. 2012, AJ, 144, 155
Smirnova, T. 2006, ARep, 50, 915
Smirnova, T. 2012, ARep, 56, 430
Smirnova, T., & Shabanova, T. 1988, SvA, 32, 61
Suleimanova, S., Volodin, Y., & Malofeev, V. 1983, SvA, 27, 322
Sutton, J. 1971, MNRAS, 155, 51
Tsai, J., Simonetti, J., Akukwe, B., et al. 2015, AJ, 149, 65
Tyul'bashev, S., Tyul'bashev, V., Kitaeva, M., et al. 2017, ARep, 61, 848
Tyul'bashev, S., Tyul'bashev, V., & Malofeev, V. 2018, A&A, 618, 70
Tyul'bashev, S., Tyul'bashev, V., Oreshko, V., & Logvinenko, S. 2016, ARep, 60, 220
Tyul'bashev, S. A., Kitaeva, M. A., Tyul'bashev, V. S., Malofeev, V. M., & Tyul'basheva, G. E. 2020, ARep, 526, 64

[1] When our manuscript was ready for submission, the preprint by Bilous et al. (astro-ph HE 2109.085 00) appeared. There some similar problems concerning variations of radiation from the pulsar B0950+08 at other frequencies (55 MHz and 1.4 GHz) are discussed. The detection of the rather strong feature between MP and IP described in this preprint is an additional argument for the aligned rotator model.